This article has been accepted for publication in a future issue of this journal, but has not been fully edited. Content may change prior to final publication. Citation information: DOI 10.1109/LAWP.2017.2702584, IEEE Antennas and Wireless Propagation Letters

Gain Improvement of Rectangular Dielectric Resonator Antenna by Engraving Grooves on its Side Walls

Saeed Fakhte, Homayoon Oraizi, *Life Senior Member, IEEE*, and Ladislau Matekovits, *Senior Member, IEEE*

***Abstract*— A new technique for increasing the boresight gain of a rectangular dielectric resonator antenna (DRA) operating at its fundamental radiating TE^{y}_{111} mode is introduced. The idea is to increase the radiations from the side walls of the DRA compared to that of its top wall, by engraving grooves on the side walls. A model based on the array theory is developed to explain the high gain nature of the antenna. The measured results demonstrate that the proposed antenna achieves an impedance bandwidth of 21% over a band of 3.24-4 GHz, with a maximum gain of 9.6 dB. This is significantly higher with respect to available data in the literature.**

***Index Terms*— Dielectric Resonator (DR), Dielectric Resonator Antenna (DRA).**

I. Introduction

DIELECTRIC resonator antennas (DRAs) have been extensively studied due to their interesting characteristics, such as wide bandwidth, lack of surface wave loss and so on [1]. The improvement of the gain of DRAs without arraying elements has been reported by various authors. In [2], the design of DRAs at high-order modes has been used as a method to improve the gain. Placing a pyramidal horn around the DRA has been proposed in [3]. In [4], a dualband DRA is introduced by splitting the DR and carving notches on it at the positions where strong electric field is present. An asymmetrical T-shaped DRA for wideband applications has been introduced in [5]. DRAs with air intrusion have already been used to enhance the impedance bandwidth [4]-[5]. However, at the authors best knowledge, no thorough study has yet been presented to determine the enhancement in directivity that can be achieved by manipulating the electric field distribution of DRA fundamental mode using air intrusions. Recently, it has been shown that by increasing the radiations from the sidewalls of a DRA operating at its fundamental mode compared to that of its top wall, the boresight gain of the antenna can be increased [6, 7].

In this paper, engraving notches on two opposite side walls of a rectangular DRA is proposed. Doing so the radiation from the corrugated surfaces compared to the top wall is augmented which in turn increases the boresight gain of the antenna. CST Microwave Studio and HFSS have been used to numerically study the modified DRA that is further fabricated and experimentally characterized.

S. Fakhte and H. Oraizi, are with the College of Electrical Engineering, Iran University of Science and Technology, Narmak, Tehran 1684613114, Iran (email: saeedfakhte@elec.iust.ac.ir, h_oraizi@iust.ac.ir).

L. Matekovits is with the Department of Electronics and Telecommunications, Politecnico di Torino, 10129 Torino, Italy, and also with Macquarie University, Sydney, NSW 2109, Australia (e-mail: ladislau.matekovits@polito.it).

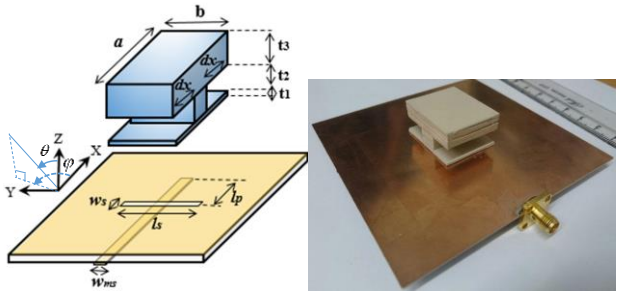

Fig. 1. 3D view of the proposed DRA configuration and its photograph.

II. Antenna Configuration

The prototype model of proposed antenna is depicted in Fig. 1, which is fabricated by placing 10 layers of a substrate with relative dielectric constant of ε_r=10.2 and thickness of 1.575 mm onto each other and pressed together mechanically. Hence, the resulting height of the DRA is *d*=15.75 mm. The other dimensions of the DRA are as follows: *a*=32 mm, *b*=26 mm, t_1=1.575 mm, t_2=6.3 mm, t_3=7.875 mm and *dx*=11 mm. The antenna is symmetrically mounted above a slot of width and length of *Ws*=2mm and *ls*=22 mm, respectively. The y-oriented slot is fed by a 50 Ω microstrip stub line of width *Wms*=1.15mm and length *lp*=16mm. It is located on the opposite side with respect to the DRA and is parallel to the *x*-direction. The microstrip line is printed on a 10×10 cm^2 substrate of thickness 0.508 mm and relative dielectric constant of ε_r=3.38. The continuous metallization on the other side also acts as ground plane for the antenna.

To gain the physical insight into the improvement of the gain, the far field E-plane (φ=0°) electric field pattern of the walls of a simple rectangular DRA in its fundamental radiating TE^{y}_{111} mode is studied. This DRA dimensions are the same as those of Fig. 1, except for the notched regions (i.e., dx=0 as illustrated in Fig. 2). This study aims to find the pair of sidewalls which produces the most directive radiation pattern in the boresight direction, i.e., $\theta = 0^o$. In a second step, by increasing the radiation intensity from these sidewalls compared to the other walls of the DRA, the overall directivity in the boresight direction can be improved.

Using the equivalence principle, the DRA is replaced by the equivalent magnetic surface current densities M_x, M_y and M_z and the electric surface current densities J_x and J_z, as shown in Fig. 2. First the radiations from the $y=\pm b/2$ walls are investigated. The vector potentials F_x and F_z due to the equivalent current densities M_x and M_z are functions of φ as follows [8]

$$F_x \propto \sin\left(\frac{k_0 b \sin(\theta)\sin(\varphi)}{2}\right) \quad (1)$$

This article has been accepted for publication in a future issue of this journal, but has not been fully edited. Content may change prior to final publication. Citation information: DOI 10.1109/LAWP.2017.2702584, IEEE Antennas and Wireless Propagation Letters

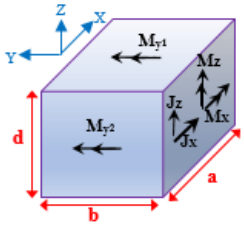

Fig. 2. 3D view of DRA by applying image theory with equivalent surface currents over its surfaces.

$$F_z \propto \sin(\frac{k_0 b \sin(\theta)\sin(\varphi)}{2}) \tag{2}$$

where k_0 is the free space wavenumber and the other parameters are defined in Figs. 1 and 2. From (1) and (2) it results that, in the φ=0 plane, the far-zone electric field radiated by the walls in $y=\pm b/2$ due to the equivalent currents M_x and M_z vanishes. Also, since the DRA has two imperfect magnetic walls at $y=\pm b/2$, the electric current densities J_x and J_z exist over these walls, unlike other walls that are perfect magnetic conductors (PMC) [1]. It is expected that the far-zone electric field generated by the equivalent electric currents J_x and J_z on the walls in $y=\pm b/2$ will be small, since their values are less significant compared to those of equivalent magnetic currents M_{y1} and M_{y2} on the other walls. Now observe in Fig. 3 that the calculated normalized far-zone E-field radiated through the $y=\pm b/2$ apertures due to the current J is 8 dB weaker than that radiated by the other apertures due to the current M_y. So, for simplicity, we assume that the radiated far-zone field in the principal E-plane (φ=0) is mostly due to the magnetic current densities, M_{y1} and M_{y2} over the $x=\pm a/2$ and $z=\pm d/2$ walls of the DRA, as shown in Fig 3.

Note that, the magnetic current densities over the $x=-a/2$ and $x=a/2$ walls have the same magnitude and phase. This is also true for the currents on the $z=-d/2$ and $z=+d/2$ walls. Observe in Fig. 4 that the magnetic current densities over these walls produce omnidirectional radiation patterns with constant radiation in the E-plane. So, the $x=\pm a/2$ walls form an array of two elements, with the same magnitude and phase, separated along the x-axis by a distance a. The array factor for the $x=\pm a/2$ walls (blue hatched sheets) along the x-axis, namely AF_x is calculated as

$$AF_x = 2\cos(k_0 \sin\theta \frac{a}{2}) \tag{3}$$

Also, for $z=\pm d/2$ walls (red hatched sheets)

$$AF_z = 2\cos(k_0 \cos\theta \frac{d}{2}) \tag{4}$$

The array factors versus θ are plotted in Fig. 5.

Because of the $\sin(\theta)$ term in (3) and the $\cos(\theta)$ term in (4), the AF_x curve shows a maximum in the boresight direction (θ=0), but the AF_z curve has a minimum in the boresight direction. So, by increasing the intensity of the magnetic current density (or z-component of electric field) over the $x=\pm a/2$ walls, $M_{y2} = E_z(x = \pm a/2, y, z)$ (blue hatched sheets) compared to that of the $z=\pm d/2$ walls (or x-component of electric field), $M_{y1} = -E_x(x, y, z = \pm d/2)$ (red hatched sheets), it is expected that the directivity of the DRA in the boresight direction will increase.

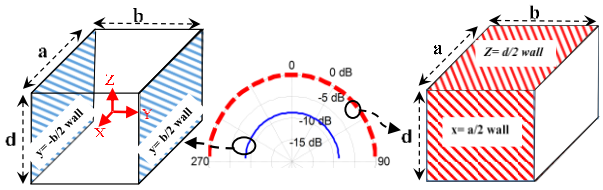

Fig. 3. E plane (φ=0) normalized electric field pattern obtained using the equivalence theory. The solid blue line is the radiated electric field due to the electric current densities on the $y=\pm b/2$ surfaces, as shown on the left side. The dashed red line is the radiated electric field due to the magnetic current densities on the $x=\pm a/2$ and $z=\pm d/2$ surfaces of the DRA, as shown on the right side. Antenna dimensions are a=32 mm, b=26 mm, d=31.5 mm, dx=0.

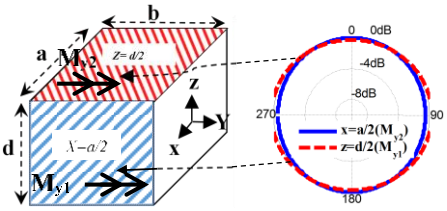

Fig. 4. E plane (φ=0) normalized electric field pattern. The solid blue line is the radiated electric field due to the magnetic current density on the $x=a/2$ wall. The dashed red line is the radiated electric field due to the magnetic current density on the z=d/2 wall.

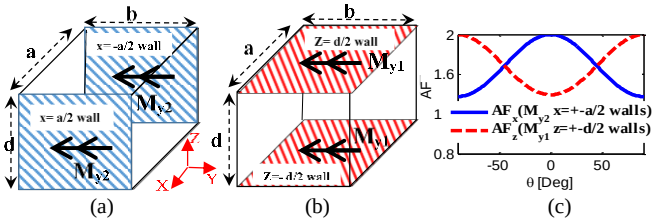

Fig. 5. Two pairs of DRA sidewalls having different array factors, (a) $x=\pm a/2$ sidewalls, (b) $z=\pm d/2$ walls, (c) array factors.

This can be further clarified by studying the total array factor of the $x=\pm a/2$ and $z=\pm d/2$ walls of the DRA. Actually, as shown in Fig. 4, each one of these walls has an omnidirectional radiation pattern and radiates like a horizontal magnetic dipole. By assuming that the $x=\pm a/2$ side walls radiate both as two horizontal magnetic dipoles with the magnitude of magnetic current density $M_{y2}(x = \pm a/2, y = 0, z = 0)$ and the $z=\pm d/2$ walls radiate both as two horizontal magnetic dipoles with the magnitude of magnetic current density $M_{y1}(x = 0, y = 0, z = \pm d/2)$, these four walls form a planar array, as shown in the inset of Fig. 6. So, the normalized array factor for this planar array is calculated as [9]:

$$AF = \frac{\cos(k_0 \cos(\theta)\frac{d}{2}) + \frac{|E_z(\pm a/2, 0, 0)|}{|E_x(0, 0, \pm d/2)|}\cos(k_0 \sin(\theta)\frac{a}{2})}{\max(\cos(k_0 \cos(\theta)\frac{d}{2}) + \frac{|E_z(\pm a/2, 0, 0)|}{|E_x(0, 0, \pm d/2)|}\cos(k_0 \sin(\theta)\frac{a}{2}))} \tag{5}$$

Note that the formula for the total radiation pattern of the antenna (E_φ pattern) is similar to (5).

Fig. 6 shows the plot of the array factor versus θ. Observe that by increasing the ratio $\frac{|E_z(\pm a/2, 0, 0)|}{|E_x(0, 0, \pm d/2)|}$, the directivity of the radiation pattern in the X0Z plane increases.

This article has been accepted for publication in a future issue of this journal, but has not been fully edited. Content may change prior to final publication. Citation information: DOI 10.1109/LAWP.2017.2702584, IEEE Antennas and Wireless Propagation Letters

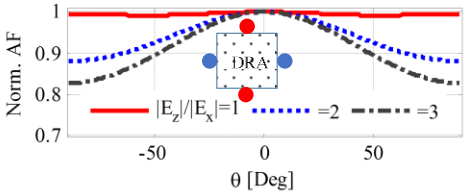

Fig. 6. Normalized array factor for $x=\pm a/2$ and $z=\pm d/2$ walls of the DRA. The XZ view of the antenna and magnetic dipoles are shown in the inset.

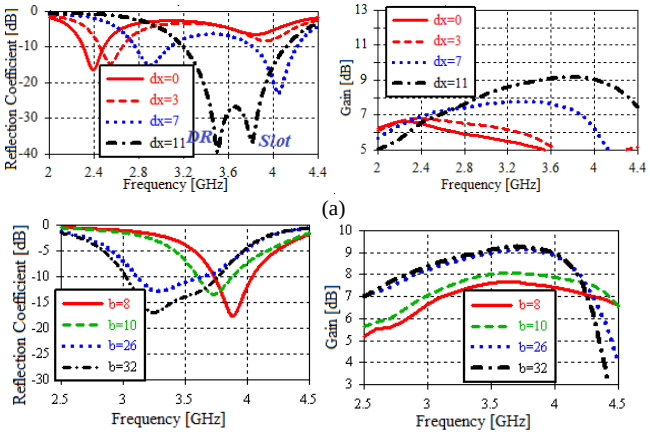

Fig. 7. Simulated (CST) reflection coefficient and gain for (a) various notch depth, *dx*, (b) various DRA widths, *b*.

III. PARAMETRIC STUDY

A parametric study of the proposed antenna has been carried out. Fig. 7(a) shows the magnitude of reflection coefficient and gain for different notch depths, *dx*. Observe that increasing the notch depth will significantly increases the lower resonance frequency but its effect on the upper resonance is rather small. These results provide the evidence that the upper resonance frequency is due to the coupling slot but the lower one is due to the DRA radiation mode. Also, when the depth *dx* increases, the gain increases due to the increase in magnitude of the electric field in the notch regions.

Fig. 7(b) shows the results for different DRA width, *b*. Observe that the impedance matching condition changes considerably. Also, by decreasing the DRA width, the DRA gain is decreased. One can explain this by considering the change in the areas of the DRA walls. Consider the aforementioned standard rectangular DRA without notches. With reference to Figs. 3, by decreasing the width, the radiation apertures of the $x=\pm a/2$ and $z=\pm d/2$ walls are decreased, but those of the $y=\pm b/2$ walls are kept constant. On the other hand, it can be shown, e.g. using dielectric waveguide model [1], that by decreasing the b/a ratio, the tangential magnetic field strength over the $y=\pm b/2$ walls will be increased, which can be interpreted as the increase in the electric current densities J_x and J_z over the $y=\pm b/2$ walls. Observe in Fig. 8, for b=10 mm, the far-zone E-field due to J over the $y=\pm b/2$ walls is 2 dB stronger than that of M over the other walls. So, the contribution of J_x and J_z over the $y=\pm b/2$ walls compared to those of the magnetic current densities over the other walls, to the overall radiation pattern will be increased. This can be seen from the comparison of Figs. 3 and 9. So, unlike the previous case in Fig. 3 with b=26 mm, the J

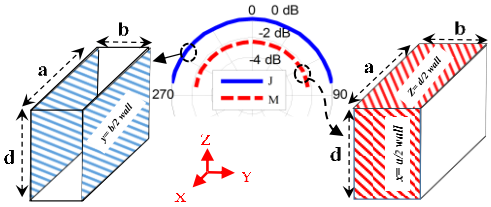

Fig. 8. E plane (φ=0) normalized electric field pattern obtained using the equivalence theory.

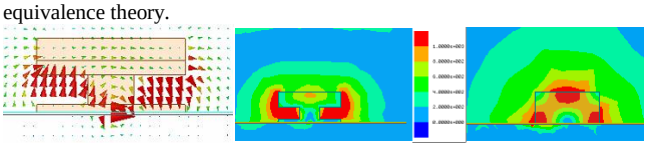

Fig. 9. Simulated (HFSS) electric field distribution: (a) vector plot at 3.5 GHz., X0Z plane. (b) magnitude plot of DRA with notches (dx=11 mm) at 3.5 GHz., X0Z plane (c) magnitude plot of DRA without notches (dx=0) at 2.4 GHz., X0Z plane.

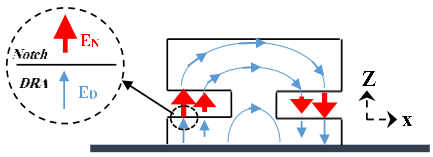

Fig. 10. Electric field distribution of the proposed DRA at 3.5 GHz.

effect is considerable on the radiation pattern (solid blue line in Fig. 8). So, narrowing the main beam of radiation pattern due to M (dashed red line in Fig. 8) by engraving grooves, cannot considerably affect the total radiation pattern of the DRA. Therefore, it is expected that engraving notches on the sidewalls of a rectangular DRA with a narrow width, *b*, has no considerable effect on the gain of the DRA, as shown in Fig. 7(b).

The electric field distribution of the proposed DRA at 3.5 GHz is shown in Figs. 9(a) and (b). This resembles the TE^{y}_{111} mode of the rectangular DRA. The electric field magnitude plot of a standard DRA with the same dimensions as the proposed DRA (without notches dx=0) is compared with those of the proposed DRA (with notches dx=11 mm) in Figs. 9(b) and (c). Note that in Fig. 9(c), the strength of electric fields on $z=d/2$ and $x=\pm a/2$ walls are the same, but in Fig. 9(b) the electric field on the $x=\pm a/2$ walls is stronger than those on the $z=d/2$ wall.

Observe in Fig. 10 that, the strength of the E_z component normal to the air-dielectric interface in the notch regions is enhanced to satisfy the continuity condition [4].

IV. MEASURED RESULTS

The simulated and measured reflection coefficient of the proposed DRA are plotted versus frequency in Fig. 11. Some discrepancies between the measured and simulated reflection coefficients are observed, which may be attributable to the inaccuracies in fabrication process comprising stacking ten thin dielectric layers and pressing them together mechanically and also to the possible presence of air gaps between the layers and between the ground plane and the bottom of DRA. Note that the measurement predicts a 10-dB impedance bandwidth over 3.24-4 GHz.

This article has been accepted for publication in a future issue of this journal, but has not been fully edited. Content may change prior to final publication. Citation information: DOI 10.1109/LAWP.2017.2702584, IEEE Antennas and Wireless Propagation Letters

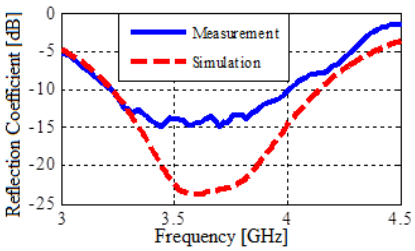

Fig. 11. Measured and simulated (CST) reflection coefficients of the proposed DRA.

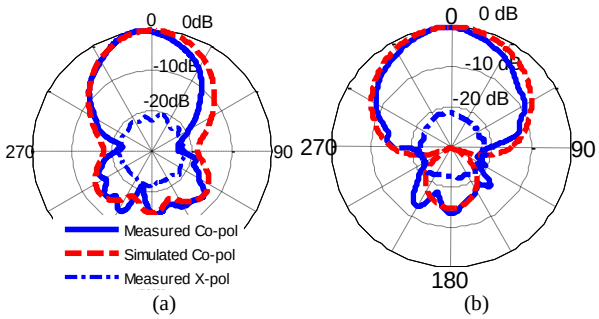

Fig. 12. Simulated (CST) and measured normalized radiation patterns at 3.5 GHz for the proposed DRA (a) in the X0Z plane, (b) in the Y0Z plane.

Fig. 12 shows the simulated and measured normalized radiation patterns of the proposed antenna in the X0Z- and Y0Z-planes at 3.5 GHz. In both planes broadside radiation patterns are observed. Fig. 13 shows the simulated and measured gain versus frequency. Observe that both gains are higher than 8.5 dB over the whole operating band. Also, note that the measured gain reaches the maximum value of 9.6 dB at 3.5 GHz. This is approximately 3.6 dB above the typical gain of a rectangular DRA operating at its fundamental mode. Also observe in Fig. 13 that, the simulated radiation efficiency is more than 94% over the 10 dB reflection coefficient band.

V. Discussion

Finally, the proposed antenna is compared with the similar reported structures in [4] and [5]. Unlike works in [4] and [5] where the high gain nature of the DRA in the upper band is due to the presence of the higher order mode [2], here the possibility to improving the boresight gain of DRA operating in its fundamental TE^{y}_{111} mode is investigated. In [4], two notches are engraved at the side edges of the DRA with relatively low depths (*dx* in Fig. 1) and one notch is engraved on the top wall of the DRA which are the main differences of the aforementioned work with the present work. On the other hand, in [4] only the effect of notches on the impedance bandwidth and resonant frequencies are discussed. The measured gain of this antenna in its fundamental TE^{y}_{111} mode is about 3 dB lower than the gain achieved in the present work.

The study in [5] has only focused on the miniaturization and impedance matching of the antenna. The measured gain of asymmetrical T-shaped DRA at the fundamental TE^{x}_{111} mode resonance frequency is around 5.5 dB, which is 4 dB lower than the gain achieved in the present work. In [5], the DRA width *b* is very narrow compared to its length *a* (width-to-length ratio ≈ 0.29), unlike our structure where this ratio is 0.81. The dependency of the gain to DRA width is confirmed by a parametric study in our work (see Fig. 7(b) and Fig. 8). Also, the electric field distribution in the notched region is significantly affected by the presence of metallic probe, unlike the aperture feed coupling used in our design.

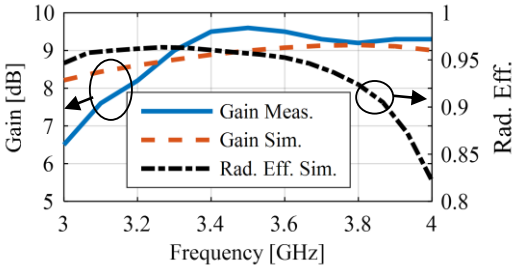

Fig. 13. Gain and radiation efficiency of the proposed antenna.

VI. Conclusion

A novel technique is presented for gain enhancement of rectangular DRA based on the manipulation of the electric field distribution within the resonator. By increasing the radiation from its sidewalls compared to its top wall, the directivity can be improved significantly. The concept is theoretically proved and verified by comparing the simulation and measured results.

References

[1] R. K. Mongia and A. Ittipiboon, "Theoretical and experimental investigations on rectangular dielectric resonator antennas," *IEEE Trans. Antennas Propag.*, vol. 45, pp. 1348–1356, 1997.

[2] A. Petosa and S. Thirakoune, "Rectangular Dielectric Resonator Antennas with Enhanced Gain," *IEEE Transactions Antennas and Propagation*, vol. 59, pp. 1385 - 1389, 2011.

[3] Nasmuddin and K. P. Esselle, "Antennas with dielectric resonators and surface mounted short horns for high gain and large bandwidth," *IET Proc. Microw., Antennas Propag.*, vol. 1, no. 3, pp. 723–729, Jun. 2007.

[4] T. H. Chang and J. F. Kiang, "Dual-band split dielectric resonator antenna," *IEEE Trans. Antennas Propag.*, vol. 55, no. 11, pp. 3155–3162, Nov. 2007.

[5] Y. Gao, Z. Feng, and L. Zhang, "Compact Asymmetrical T-Shaped Dielectric Resonator Antenna for Broadband Applications," *IEEE Trans. Antennas Propag.*, vol. 60, no. 3, pp. 1611–1615, Mar. 2012.

[6] S. Fakhte, H. Oraizi and L. Matekovits, "High Gain Rectangular Dielectric Resonator Antenna Using Uniaxial Material at Fundamental Mode," in *IEEE Trans. Antennas and Propag.*, vol. 65, no. 1, pp. 342-347, Jan. 2017.

[7] S. Fakhte, H. Oraizi, L. Matekovits and G. Dassano, "Cylindrical Anisotropic Dielectric Resonator Antenna With Improved Gain, " in *IEEE Trans. Antennas and Propag.*, vol. 65, no. 3, pp. 1404-1409, March 2017.

[8] S. Maity, and B. Gupta, "Closed Form Expressions to Find Radiation Patterns of Rectangular Dielectric Resonator Antennas for Various Modes," *IEEE Trans. Antennas Propag.*, vol. 62, no. 12, pp. 6524–6527, 2014.

[9] W. L. Stutzman and G. A. Thiele, Antenna Theory and Design, 3rd ed. New York: Wiley, 2012, p. 312.